

POROSITY EVOLUTION OF FREE AND CONFINED BENTONITES DURING INTERLAYER HYDRATION

WILLIAM J. LIKOS¹ AND ALEXANDRA WAYLLACE²

¹ University of Missouri-Columbia, Department of Civil and Environmental Engineering, Columbia, MO 65211, USA

² Colorado School of Mines, Engineering Division, Golden, CO 80401, USA

Abstract—Methods for predicting the volume change and swelling-pressure behavior of expansive clays require detailed understanding of coupled interactions between clay microstructure and macrostructure under hydraulic, thermal, and mechanical loads. In this study a suite of water-vapor sorption experiments was conducted using compacted bentonites hydrated in controlled relative humidity (RH) environments maintained under free and constrained volume-change boundary conditions. Emphasis was placed on examining the influences of compaction and predominant exchange cation on the water uptake, volume change, and swelling pressure response. Densely compacted specimens exhibited greater volume changes under free swelling conditions and greater swelling pressures under fully confined conditions. Water uptake, volume change, and swelling pressure were all more significant for Colorado (Ca²⁺/Mg²⁺) bentonite than for Wyoming (Na⁺) bentonite. Plastic yielding, evident as a peak in the relationship between swelling pressure and RH, was more evident and occurred at lower RH for the Colorado bentonite. This observation was interpreted to reflect the limited capacity for interlayer swelling in Ca²⁺/Mg²⁺ bentonites and corresponding structural collapse induced by the onset of water uptake in larger intra-aggregate and inter-aggregate pores. A semi-quantitative model for the evolution of clay microstructure resulting from interlayer hydration was considered to attribute the experimental observations to differences in the efficiency with which transitions in basal spacing translate to bulk volume changes and swelling pressure. Results provide additional insight and experimental evidence to more effectively model the mechanical behavior of compacted bentonites used as buffer or barrier materials in waste repository applications.

Key Words—Bentonite, Dehydration, Hydration, Interlayer Swelling, Smectite, Sorption.

INTRODUCTION

A significant amount of recent research has focused on developing methodologies for predicting the short- and long-term behavior of compacted expansive clays used as buffer or barrier materials for waste repositories, most notably in the context of high-level radioactive waste disposal (e.g. Pusch, 1994). Central to most of these efforts is recognition of the need to consider the role of clay particle and pore structure (fabric) in governing the bulk clay behavior. In particular, features of the pore fabric existing on multiple levels of scale (typically termed the microstructure and macrostructure) clearly must be explicitly considered. The micro and macrostructures of compacted clay interact and evolve in a coupled fashion as hydraulic, thermal, or mechanical loading processes occur. This ultimately translates into volume change, swelling pressures, and/or hydrologic changes measurable on the bulk scale. The extent of these changes, however, is highly dependent on multiple factors, including the initial fabric, compaction density, water content, pore-water potential, confining stress, wetting history, and the hydraulic, thermal, chemical, and mechanical boundary conditions applied.

Techniques such as mercury intrusion porosimetry (MIP) and environmental scanning electron microscopy (ESEM) are providing key qualitative and quantitative insight into compacted clay fabric, its evolution under various types of loading, and the corresponding impact on clay behavior (e.g. Romero and Simms, 2008). Various forms of double-structure models have been proposed to relate changes in clay microstructure and macrostructure to the bulk material response, including models for mechanical response such as swelling pressure or volume change (Gens and Alonso, 1992; Alonso *et al.*, 1999; Cui *et al.*, 2002), hydrologic response such as water conduction or retention behavior (Tuller and Or, 2003), and complex thermo-mechanical-hydraulic behavior applicable to many waste-disposal applications (e.g. Sánchez *et al.*, 2005).

Continued advancement of these types of models requires refinement of our basic understanding of how clay microstructure and macrostructure evolve for various initial, loading, and boundary conditions, and how this evolution translates into bulk behavior. Experimental constraints on this behavior, however, currently remain significantly limited, a restriction due in large part to the considerable difficulties and time requirements necessary to make robust measurements (Lloret *et al.*, 2003). The present authors previously presented results from a suite of controlled relative-humidity swelling tests for compacted bentonites

* E-mail address of corresponding author:

likosw@missouri.edu

DOI: 10.1346/CCMN.2010.0580310

maintained under free swelling (unconfined) boundary conditions (Likos and Lu, 2006). Results were interpreted using a simple pore-scale model proposed to quantify the evolution of clay microstructure resulting from sequential hydration of water layers in the expandable mineral interlayers. Here a detailed experimental program including measurements of bulk-volume changes and swelling pressures for bentonites hydrated under free swelling and fully confined (zero-volume-change) boundary conditions is reported. Emphasis is placed on examining the influences of compaction density (void ratio) and predominant exchange cation (Na^+ vs. $\text{Ca}^{2+}/\text{Mg}^{2+}$) on measured water uptake, volume change, and swelling-pressure response. Observations are interpreted in light of results from the limited suite of similar measurements available in the literature and the Likos and Lu (2006) porosity-evolution model.

MATERIALS AND METHODS

Bentonite characteristics and preparation

Two types of bentonite were selected for testing: a commercial Wyoming bentonite and a naturally occurring bentonite sampled from an outcrop of the Graneros shale in Golden, Colorado, USA. Cation exchange capacity (CEC) and exchangeable cations were measured using two procedures (USDA, 2004). The ammonium acetate method (pH 7) was used for exchangeable cations and CEC measurements. Exchangeable cations were also determined using the unbuffered ammonium chloride procedure for comparison. The CEC values determined using the ammonium acetate method were 66 meq/100 g and 82 meq/100g for the Wyoming bentonite and Colorado bentonite, respectively

(Table 1). Results for exchangeable cations differed markedly for both procedures. Ammonium chloride results indicate that 59% Na^+ , 36% Ca^{2+} , 5% Mg^{2+} , and <1% K^+ are present in the Wyoming bentonite and 3% Na^+ , 59% Ca^{2+} , 38% Mg^{2+} , and <1% K^+ in the Colorado bentonite. Ammonium acetate results yield more Na^+ (67%) for the Wyoming bentonite and less Mg^{2+} (30%) for the Colorado bentonite. The reasons for these differences are unknown. While good agreement was obtained for exchangeable K^+ and Ca^{2+} , exchangeable Ca^{2+} is believed to be inflated at least for the Wyoming bentonite because typically this bentonite contains traces of calcite and/or gypsum which are known to be dissolved partly during CEC determination (e.g. Dohrmann and Kaufhold, 2009). Nevertheless, the Colorado bentonite is saturated largely (>95%) by divalent cations, whereas Wyoming bentonite contains a minimum of 60% monovalent cations. Relatively large liquid and plastic limits ($w_l = 485\%$, $w_p = 132\%$) for the Wyoming bentonite reflect the predominance of Na^+ in the exchange complex. Smaller values for the Colorado bentonite ($w_l = 118\%$, $w_p = 45\%$) reflect the predominance of divalent Ca^{2+} and Mg^{2+} .

X-ray diffraction (XRD) results obtained for bulk powder and clay-size fraction samples (Likos and Lu, 2006) indicated that the Wyoming bentonite consisted predominantly of discrete smectite with minor kaolinite, quartz, and zeolite. Smectite percentage ranges from 75 to 100% for typical commercial-grade Wyoming bentonite. The Colorado bentonite was primarily discrete smectite with trace kaolinite and non-clay minerals. The smectite percentage ranges from 95 to 100% of the clay fraction and 65–100% of the whole rock for similar bentonite beds characteristic of the Colorado Front

Table 1. Mineralogy and index properties of test materials.

Property		Wyoming bentonite	Colorado bentonite
Mineralogy ^a		S, K, Qtz, zeolite	S, K, Qtz, calcite, feldspar
	Total CEC	66	82
	Na^+	59%	3%
Cation exchange capacity ^b (meq/100 g)	K^+	<1%	<1%
	Ca^{2+}	36%	59%
	Mg^{2+}	5%	38%
Crystallite thickness ^c (nm)		12.7	11.1
	w_l (%)	485	118
Atterberg limits ^d	w_p (%)	132	45
	PI	353	73
% Clay size (<2 μm)		70–90 ^e	90
USCS classification		CH	CH

^a S = smectite, K = kaolinite; determined by XRD using $\text{CuK}\alpha$ radiation

^b CEC determined by the 1 N ammonium acetate method, % extractable bases by 1 N ammonium chloride method

^c determined using the *MudMaster* program for glycolcated XRD patterns, smectite 001 reflection (Eberl *et al.*, 1996)

^d ASTM D4318 (ASTM, 2000), PI = plasticity index = $w_l - w_p$

^e assumed as typical value for commercial-grade Wyoming bentonite.

Range sampling location (Noe *et al.*, 2007). Typically, smectites of Wyoming bentonites are low-charged but no such data are available for the Colorado bentonite. Mean thicknesses of the smectite crystallites were estimated using the Fourier decomposition technique of Bertaut-Warren-Averbach applied to XRD patterns obtained for the glycolated clays (Eberl *et al.*, 1996). Mean crystallite thicknesses were 12.7 nm and 11.1 nm for the Wyoming and Colorado bentonites, respectively, corresponding to a mean of 7.6 and 6.6 expandable layers per crystallite, respectively. The particle density of the mineral solids (G_s) was assumed to be 2.70 g/cm³ for subsequent porosity calculations in both cases.

The Colorado bentonite was air-dried after field sampling and pulverized by gentle grinding to pass through a 75 μm (#200) sieve. Compacted specimens were prepared from the pulverized material for subsequent water-vapor sorption and swell testing. The Wyoming clay was supplied in powdered form (<75 μm) and not processed prior to compaction. A Ca²⁺-exchanged form of the Wyoming bentonite was prepared by washing it (~1 g) five times in suspension with (~50 mL) 0.1 M CaCl₂, followed by repeated washings with distilled water until excess chloride ions were removed as detected by AgNO₃ (Moore and Reynolds, 1997).

Scanning electron microscopy (SEM) images were obtained using an FEI Quanta 600 instrument for samples compacted to an initial dry density of 1.5 g/cm³. Specimens were dried and split by hand to obtain images on the fresh surface of the split cross section after platinum sputtering. Images (*e.g.* Figure 1a) confirmed the existence of bimodal porosity comprising inter-aggregate pores that ranged in size from ~10 μm to 100 μm and intra-aggregate pores ranging from ~0.1 μm to 1 μm . This bimodal or double-structure and corresponding range of pore sizes are consistent with previous qualitative and quantitative observations from SEM, MIP, and other microstructural fabric studies for variously compacted Na⁺ and Ca²⁺/Mg²⁺ bentonites (*e.g.* Romero and Simms, 2008).

As illustrated conceptually in Figure 1, pores comprising the smaller-scale microstructure of compacted bentonites are generally designated as those corresponding to interlayer separations between expandable mineral layers (Figure 1e), discontinuities between oriented sub-stacks of mineral layers (Figure 1d), and intra-aggregate voids formed within the larger aggregates of clay particles (Figure 1c). These particles, or quasicrystals (Aylmore and Quirk, 1971), contain multiple oriented sub-stacks of mineral layers to form network walls within the clay aggregates. Pores comprising the macrostructure are generally considered to be those formed among the aggregates, also referred to as the inter-aggregate void space (Figure 1b). These general designations are retained in subsequent discussion of the sorption, free-swelling, and confined-swelling test

results. In addition, the Likos and Lu (2006) porosity-evolution model used to interpret the confined-swelling results differentiates an interlayer void space and corresponding interlayer void ratio (e_{il}) from a more broadly defined interparticle void space and interparticle void ratio (e_{ip}). The interparticle void space is the sum of the intra-aggregate and inter-aggregate voids (Figure 1b). Water uptake for RH conditions of <~95% RH occurs primarily as an expansion of interlayer spacing (2δ) within expandable mineral interlayers with concurrent adsorption on external mineral surfaces in both the intra-aggregate and inter-aggregate pores. Changes in volume occurring on the interlayer scale translate to bulk-volume change and swelling pressure measurable at the bulk scale with efficiency dependent on the compaction-dependent fabric of the clay and the boundary conditions applied.

Free swell testing

Specimens for free swell testing were prepared by compressing ~10 g of oven-dried (105°C) clay into a lubricated 3.78 cm diameter cylindrical mold using a 50 kN load frame. Specimens were extruded from the mold using a piston assembly and oven dried at 105°C a second time to constant mass. Likos and Lu (2006) reported detailed relationships between compaction pressure and corresponding total void ratio for these two clays. For the current test program, this resulted in a suite of compacted specimens with void ratio (e) ranging from 1.30 to 0.70 and corresponding dry density (γ_d) ranging from 1.2 g/cm³ to 1.6 g/cm³. (Void ratio (e) is defined as $e = V_v/V_s$, where V_v = void volume and V_s = solids volume. Porosity (n) is defined as $n = V_v/V_t$, where V_t is the total volume.) The initial specimen height ranged from 0.54 to 0.80 cm and averaged 0.66 cm, resulting in an average specimen volume for free and confined swelling testing of 7.41 cm³. These relatively thin specimens were prepared to reduce the effects of side-wall friction in the confined-swelling tests and to reduce the amount of time required for steady-state water uptake and volume change to be reached.

Water-vapor-sorption isotherms and corresponding bulk-volume changes were measured by equilibrating the clays in controlled-humidity environments maintained in the headspace of environmental chambers using saturated salt solutions (Table 2). The RH- and temperature-correction coefficients for each solution were taken from Young (1967). Corresponding total suction values (ψ_t) were calculated using Kelvin's psychrometric law. Sorption isotherms were obtained along a 9-step hydration path by cycling the specimens through each environmental chamber, starting with the first chamber containing desiccant (silica gel) at 5% RH and progressively ramping up through to the final chamber containing a saturated solution of K₂SO₄ at 97% RH. Equilibrium at each increment was determined by measuring the sample mass periodically until steady

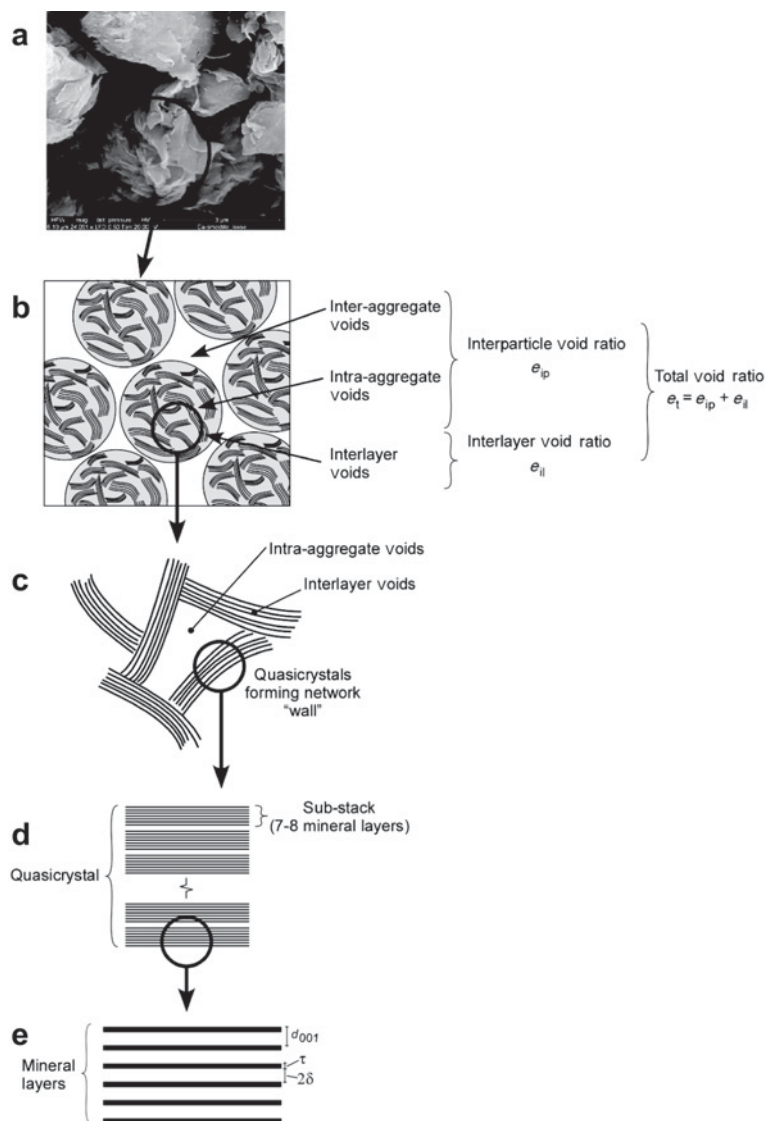


Figure 1. SEM image (a) of compacted Wyoming bentonite showing bimodal porosity (image obtained parallel to compaction direction). Parts b–e are conceptual diagrams of pore spaces on the (b) inter-aggregate scale, (c) intra-aggregate scale, (d) quasicrystal scale, and (e) interlayer scale.

Table 2. Summary of salt solutions used for humidity control in free swelling tests. RH and temperature coefficient values are from Young (1967).

Saturated salt solution	RH at 25°C (%)	$d(\text{RH})/dT$ (%RH/C)	Total suction, ψ_t (MPa)
Desiccant	5.0*	–	405
NaOH.H ₂ O	7	0.00	359
LiCl.H ₂ O	11.3	–0.01	294
MgCl ₂ .6H ₂ O	32.7	–0.06	151
MgNO ₃	52.8	–0.29	86
NaBr.2H ₂ O	58.2	–0.28	73
NaCl	75.1	–0.02	39
KCl	84.2	–0.16	23
K ₂ SO ₄	97	–0.15	4

* measured using thin-film capacitance hygrometer.

state was reached. An equilibration period of 48 to 72 h was typically required for each step, requiring ~30 days to complete the 9-step hydration cycle. Gravimetric water content ($w = m_w/m_s \times 100\%$; m_w = water mass, m_s = dry solids mass) and axial strain ($\epsilon_a = \Delta h/h_i \times 100\%$; Δh = change in specimen height, h_i = initial specimen height) were computed at steady state by measuring the mass and height of the specimens to a resolution of 0.0001 g and 0.0001 cm, respectively. Specimen mass was measured by removing the specimen from the chamber and placing it on an electronic balance. Specimen height was measured using a micrometer assembly. Radial-specimen deformations required to compute bulk volume changes were not measured but rather were inferred by assuming that volume change under free-swelling conditions is isotropic and that the radial and axial strain are equal (e.g. Delage *et al.*, 1998). Tests were conducted at an average temperature of 23.9°C with a standard deviation measured among the various chambers of 0.3°C.

Materials prepared for free-swell testing included three specimens of the Wyoming bentonite compacted to representative dense ($e = 0.88$, $\gamma_d = 1.44 \text{ g/cm}^3$), moderate ($e = 1.10$, $\gamma_d = 1.29 \text{ g/cm}^3$), and loose ($e = 1.28$, $\gamma_d = 1.19 \text{ g/cm}^3$) conditions (one specimen was tested at each density). Three specimens of the Colorado bentonite were compacted to representative dense ($e = 0.74$, $\gamma_d = 1.55 \text{ g/cm}^3$), moderate ($e = 0.83$, $\gamma_d = 1.47 \text{ g/cm}^3$), and loose ($e = 0.92$, $\gamma_d = 1.41 \text{ g/cm}^3$) conditions. One specimen of the Ca^{2+} -exchanged Wyoming bentonite was also tested at an initial void ratio of $e = 0.88$ for direct comparison with similarly compacted specimens of the unprocessed Wyoming and Colorado clays (*i.e.* those compacted to $e = 0.88$ and $e = 0.83$, respectively).

Confined-swell testing

Confined-swell tests were conducted in an apparatus (Figure 2) developed by integrating a controlled-humidity environmental chamber (Likos, 2004) with a

computer-automated, one-dimensional load frame capable of maintaining constant load or deformation conditions (Geotac Soil Testing Equipment, Houston, Texas, USA). Relative humidity was actively controlled from a minimum of ~1% RH to a maximum of ~95% RH by proportioned mixing of vapor-saturated and dry-air streams (Hashizume *et al.*, 1996; Chipera *et al.*, 1997). Lateral specimen deformation was prevented by using a confining ring with an inner diameter of 3.71 cm. Specimen height varied depending on the initial specimen density and averaged ~0.7 cm. Perforated disks and grooved spacers were placed on top and bottom of the specimen to allow it to come to equilibrium with water vapor in the chamber.

Confined-swell testing results were obtained for two specimens of the Wyoming bentonite initially compacted to void ratios of 0.75 (1.54 g/cm^3) and 0.87 (1.44 g/cm^3) to represent relatively dense and loose conditions, respectively. Two specimens of the Colorado bentonite were compacted to void ratios of 0.75 (1.54 g/cm^3) and 1.14 (1.26 g/cm^3). All specimens were initially oven dried to constant mass at 105°C, compacted to target void ratio directly in the confining ring in the chamber, subjected to a dry (~1% RH) air stream for several days, brought to an initial seating pressure of 40 kPa, and then subjected to increasing RH increments along a multistep hydration path. Increments continued to a maximum of ~95% RH in steps of ~10% RH. Humidity was measured continuously and logged during testing using a thin-film capacitance probe calibrated prior to testing using saturated salt solutions. Zero-volume-change conditions were maintained using the confining ring and the automated loading frame. Corresponding swelling pressure was measured and monitored for steady state using a strain-gauged load cell integrated into the loading ram. Swelling pressure was measured to a resolution of 8 kPa, corresponding to 0.5% to 2.0% of the full scale range for a typical test. A complete hydration cycle included 8 to 10 RH increments and required 5 to 7 months to complete.

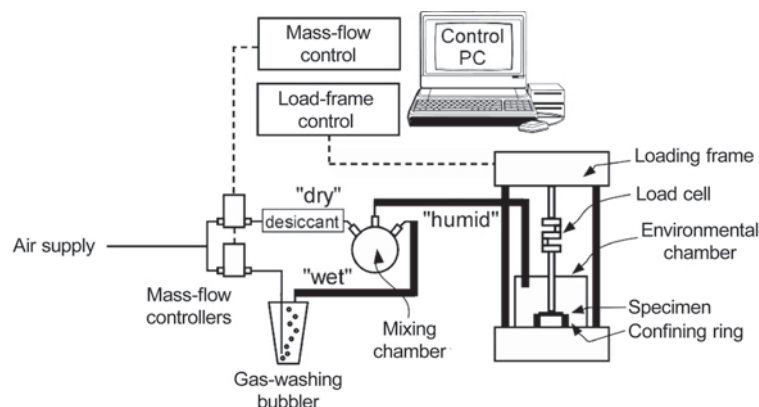


Figure 2. Schematic diagram of the experimental system for humidity-controlled swelling-pressure tests conducted under zero-volume-change (fully confined) boundary conditions.

RESULTS AND DISCUSSION

Sorption behavior under free swelling conditions

Water-vapor sorption isotherms obtained for the variously compacted specimens under free swelling conditions were found to be essentially independent of initial compaction density over the majority of the measured RH range (Figure 3). The difference in water content among either the three preparations of Wyoming bentonite or the three preparations of Colorado bentonite for RH values <97% did not exceed $w \pm 1.5\%$. Some deviation was observed at the highest increment (RH = 97%), where the densest preparations adsorbed less water than the moderate and loose preparations, which remained comparable.

Similar observations of the water-vapor-sorption behavior of free and confined bentonites have been

made by a number of previous studies. For example, Villar (2007) measured the water retention behavior of two fully confined bentonites prepared to initial dry densities ranging from 1.30 g/cm^3 to 1.70 g/cm^3 , including a predominantly Na^+ bentonite (MX-80) and a predominantly $\text{Ca}^{2+}/\text{Mg}^{2+}$ bentonite (FEBEX) similar to the Wyoming and Colorado bentonites examined here. Differences in water uptake were found to be negligible for RH values of $< \sim 92\%$ ($\psi_t > 10 \text{ MPa}$). Loosely compacted preparations adsorbed more water at greater RH values, an observation interpreted to reflect the greater amount of pore volume available for water uptake in the looser samples.

The general interpretation in those studies and here is that, at low RH, water is retained by the smaller interlayer and intra-aggregate pores and is thus governed by the surface and charge properties of the mineral

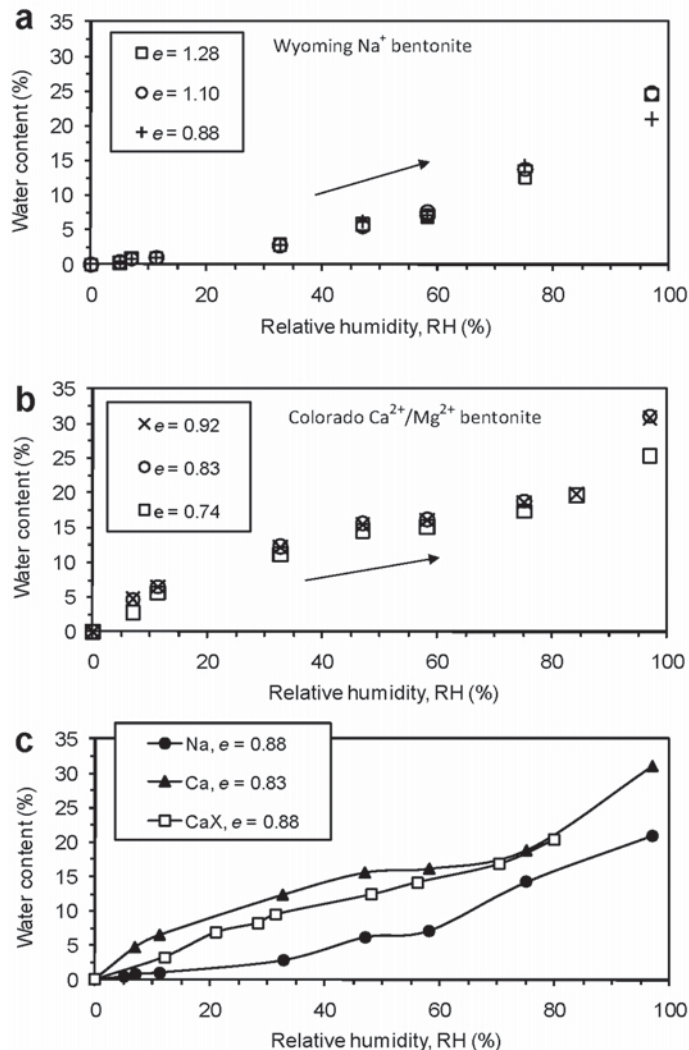


Figure 3. Water-vapor sorption isotherms for specimens compacted to various initial void ratio (e): (a) Wyoming bentonite, (b) Colorado bentonite, (c) Wyoming, Colorado, and Ca^{2+} -exchanged Wyoming bentonite (denoted CaX).

surfaces rather than the larger-scale features of the pore fabric. At higher RH, mechanisms for water-uptake transition into a regime dominated by capillary condensation in the larger-scale pores. Water uptake and retention behavior thus becomes more sensitive to the geometric features of the pores, which are readily modified by compaction. Conditions that constrain or decrease the volume of the larger pores, such as high initial density, high confining pressure, or fully constrained swelling, result in a decreased capacity for continued water uptake in this regime. Previous investigations, for example, have also shown that water-uptake behavior depends on confining stress, where, in general, a greater amount of water was adsorbed if the sample was free to swell than if volume change was constrained, but this effect was most notable at higher RH (e.g. Yahia-Aissa *et al.*, 2001; Al-Mukhtar *et al.*, 1999; Villar, 2007).

The amount of water adsorbed by the Colorado bentonite at an initial void ratio of 0.83 under free swelling conditions was significantly greater than that for the similarly compacted ($e = 0.88$) specimen of Wyoming bentonite (Figure 3c). The Colorado bentonite also adsorbed slightly more water than the similarly compacted Ca^{2+} -exchanged (CaX) Wyoming bentonite for RH $< \sim 70\%$, but water uptake at higher RH was very similar. These observations are consistent with previous measurements of water sorption for expansive clays under free swelling and confined swelling conditions (e.g. Mooney *et al.*, 1952; Keren and Shainberg, 1975; Keren and Shainberg, 1979; Hall and Astill, 1989; Berend *et al.*, 1995; Saiyouri *et al.*, 2004; Villar, 2007). Studies using homo-ionic smectites, for example, have shown that water uptake increases with increasing ionic potential of the exchange cation in the general order $\text{Na}^+ < \text{Ca}^{2+} < \text{Mg}^{2+}$ (Villar, 1999). Here, BET analysis of the isotherms for RH $< 40\%$ indicated that average monolayer coverage and heat of adsorption for the three preparations of Wyoming bentonite were 26.9 mg $\text{H}_2\text{O}/\text{g}$ clay and 0.90 kcal/mole, respectively. Average monolayer coverage and heat of adsorption for the three preparations of the Colorado bentonite were larger (100.9 mg $\text{H}_2\text{O}/\text{g}$ clay and 1.26 kcal/mole), reflecting the greater energy of hydration associated with the divalent exchange complex. Monolayer coverage and heat of adsorption for the Ca^{2+} -exchanged bentonite were 85.8 mg $\text{H}_2\text{O}/\text{g}$ clay and 1.08 kcal/mole. The concave downward shape of the isotherms for the Colorado and Ca^{2+} -exchanged clays also indicates that the energy of interaction between the first mono-layer of adsorbed water molecules and the active surfaces is greater than the energy of condensation of subsequent layers (e.g. Keren and Shainberg, 1980). The concave upward shape for the Wyoming clay indicates that this difference and the corresponding hydration forces are less. The BET derived values were independent of compaction density because the sorption isotherms for

RH $< 40\%$ were essentially unaffected by compaction.

Previous studies have also shown that at RH $> \sim 95\%$, or for clays fully submerged in water, the water uptake capacity of smectites with predominantly monovalent exchange cations generally exceeds that of smectites with polyvalent exchange cations. This is attributed to the relatively weak forces of interlayer attraction in the former, which allow the interlayers to continue to adsorb water under osmotic processes after the hydration energies of the exchange cations and charge sites have been satisfied. Polyvalent systems, on the other hand, are characterized by relatively strong interlayer attractive forces and are generally constrained to a maximum of three or four interlayer water layers. Thus, water uptake at greater water content occurs primarily on external particle surfaces and within the larger-scale pore groups. This difference is readily apparent by the marked difference in liquid-limit values measured for the two clays considered here (Table 1), as well as more generally for monovalent and polyvalent smectites in the literature (e.g. Lambe and Whitman, 1969). Here, the difference in water content between the dense and loose preparations of Colorado bentonite at the greatest RH increment (Figure 3) is larger than the difference between the dense and loose preparations for the Wyoming bentonite (Figure 3a). This suggests that the sorption behavior of the Colorado bentonite at high RH is more sensitive to compaction, which may in turn reflect its limited capacity for interlayer adsorption because the predominantly divalent cation exchange complex limits the extent of interlayer dissociation. The system more readily transitions into a water uptake regime, therefore, dominated by sorption in the larger pores with a consequent sensitivity to compaction of the macrostructure. As noted subsequently, this also leads to the onset of yielding behavior in the swelling pressure response of fully confined specimens.

Volume-change behavior under free-swelling conditions

Several observations were apparent in the volume-change response measured for specimens hydrated under free swelling conditions (Figure 4): (1) unlike the water-uptake behavior, volume-change behavior for both the Wyoming and Colorado bentonites depended on compaction density; (2) the influence of compaction density appeared more systematic for the Wyoming bentonite, but more appreciable for the Colorado bentonite; (3) axial strain for the natural Colorado bentonite was significantly greater than for the Wyoming bentonite; and (4) volume changes for the dense Wyoming bentonite ($e = 0.88$) and the identically compacted Ca^{2+} -exchanged Wyoming bentonite ($e = 0.88$) were comparable for RH $< \sim 60\%$. Thereafter, the curves diverged and volume change for the Wyoming bentonite became greater.

Sequential intercalation of water layers in expandable clay interlayers occurs over RH ranging $\sim 0-90\%$ (e.g.

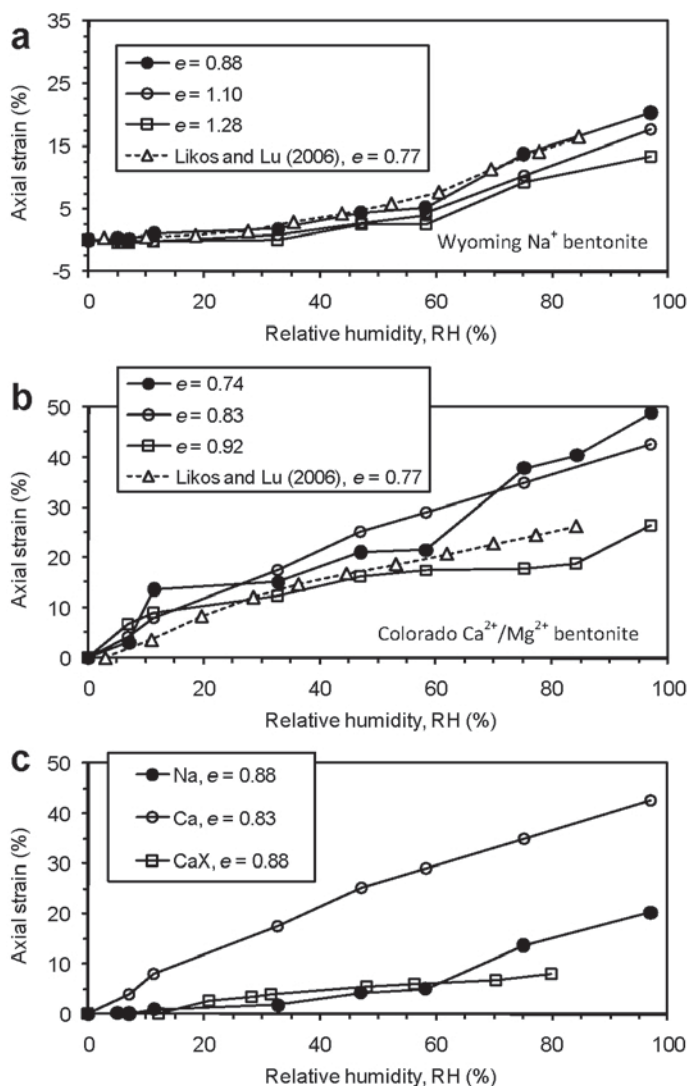


Figure 4. Axial-strain response measured along hydration paths under free swelling conditions: (a) Wyoming bentonite, (b) Colorado bentonite, (c) Wyoming, Colorado, and Ca²⁺-exchanged Wyoming bentonite (denoted CaX). Positive axial strain indicates expansion. Results from Likos and Lu (2006) are included for comparison.

Norrish, 1954). Corresponding volume changes are measurable at the interlayer scale *via* measurements of basal spacing in XRD tests (e.g. Gillery, 1959; Del Pennino *et al.*, 1981; Huang *et al.*, 1994; Chipera *et al.*, 1997; Villar, 2007) and at the bulk scale *via* swelling tests conducted under controlled humidity conditions (e.g. Bernier *et al.*, 1997; Al-Mukhtar *et al.*, 1999; Villar, 1999; Lloret *et al.*, 2003). Figure 5, for example, summarizes a suite of basal-spacing measurements determined by different researchers for predominantly Na⁺ (Figure 5a) and Ca²⁺/Mg²⁺ (Figure 5b) expansive clays. Such studies have indicated that the basal spacing of Na⁺-smectite transitions through the zero- ($d_{001} \approx 9.7 \text{ \AA}$), one- ($\sim 12 \text{ \AA}$), and two-layer ($\sim 15.5 \text{ \AA}$) hydration states when RH is increased from 0% to $\sim 90\%$. Transitions from zero-to-one and from one-to-two

water layers generally occur within RH regimes ranging from $\sim 10\text{--}30\%$ RH and $60\text{--}80\%$ RH, respectively. While multiple hydration states typically coexist (e.g. Ferrage *et al.*, 2005), interlayer spacing is relatively stable within RH domains between the transitions. In contrast, Ca²⁺- and Mg²⁺-smectites have been shown to retain one water layer at RH even approaching 0%, transition to the two-layer state by RH of about 30%, and remain stable at the two-layer state as RH approaches 90%. Transitions in basal spacing for both Na⁺ and Ca²⁺/Mg²⁺ systems also exhibit hysteresis between adsorption and desorption cycles, where larger interlayer separations are maintained to lower RH values during desorption (e.g. Chipera *et al.*, 1997; Laird *et al.*, 1995).

Observations from the suite of free-swelling experiments were interpreted in the context of basal-spacing

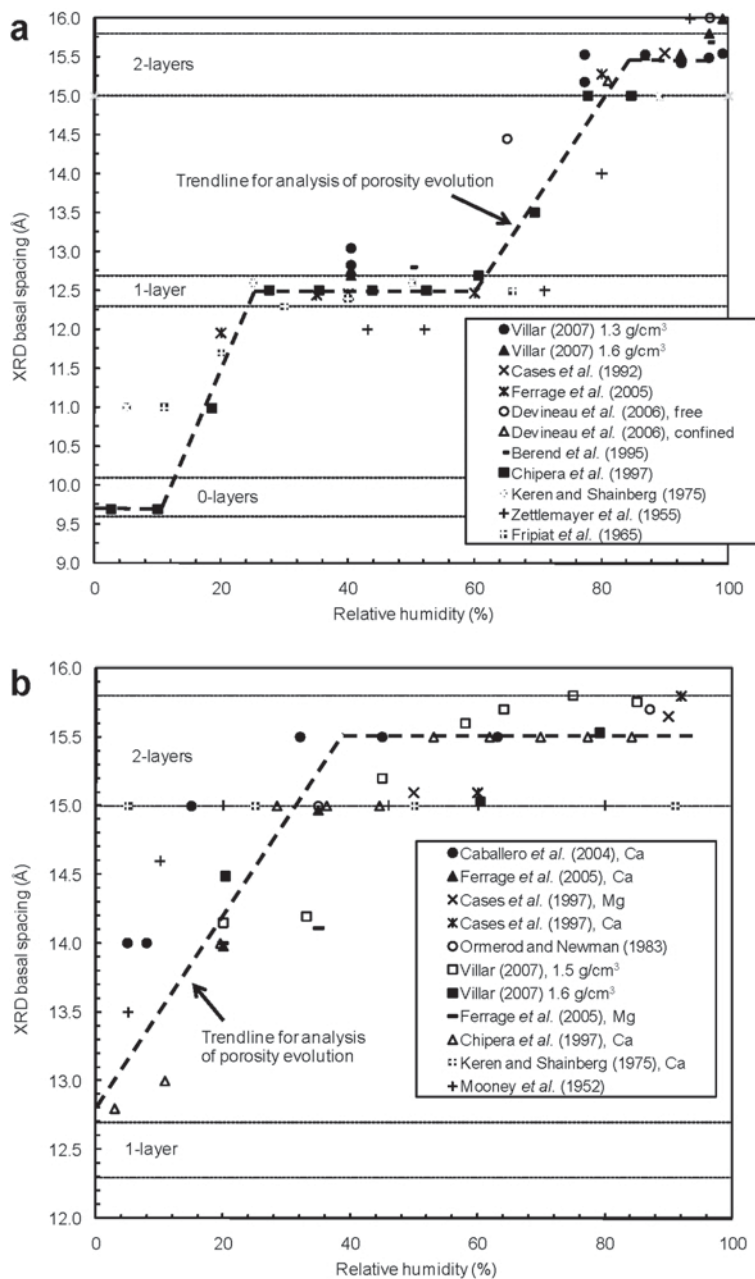


Figure 5. Summary of basal spacing measured in controlled-humidity XRD at room temperature by different authors for (a) Na^+ and (b) $\text{Ca}^{2+}/\text{Mg}^{2+}$ bentonites (after Villar, 2007). Dashed horizontal lines represent commonly reported upper and lower bounds for the two-layer hydrate condition (15.0–15.8 Å), one-layer hydrate condition (12.3–12.7 Å), and dehydrated interlayer condition (9.6–10.1 Å) (Ferrage *et al.*, 2005). Bold dashed lines are trend lines adopted for analysis of porosity evolution.

transitions associated with interlayer hydration, the interactions between clay microstructure and macrostructure, and the associated differences in fabric that result from compaction. The total porosity of compacted clay reflects contributions from the interlayer, intra-aggregate, and inter-aggregate pores. The efficiency with which particle-scale volume changes resulting from interlayer hydration translate to bulk volume changes at

the specimen scale depends on the relative volume of these internal porosities and the size and structure of the basic pore units. The nature of the interaction between the clay’s microstructural and macrostructural features depends on the state of confining stress and density. The MIP and other quantitative techniques for fabric analysis have shown that compaction by application of external pressure results primarily in compression of the larger

and more compressible inter-aggregate pores, while the less compressible intra-aggregate pores are generally unaffected (*e.g.* Lloret *et al.*, 2003). Thus, for loosely compacted specimens, the ratio of inter-aggregate pores to intra-aggregate pores is relatively large. Interlayer expansion is more effectively adsorbed by the larger pore spaces. For densely compacted specimens, the ratio of inter-aggregate pores to intra-aggregate pores decreases. Interlayer volume changes are more effectively manifest as total volume change at the specimen boundary.

The relative lack of axial strain from 0% RH to ~30% RH for the three preparations of Wyoming bentonite (Figure 4a) suggests that the volume change (expansion caused by 0-layer to 1-layer transition in basal spacing) was internally adsorbed by the larger intra-aggregate and inter-aggregate pores surrounding the particles. Volume changes within this RH range for these specimens and for the fourth, more densely compacted specimen ($e = 0.77$) from an earlier study (Figure 4a) were similar, indicating that compaction had a negligible effect within the likely regime of the 0-layer to 1-layer transition. Interlayer spacing from ~30% RH to 60% RH was probably relatively stable, yet water contents increased from an average of 3% to 7% (Figure 3a) and a small amount of bulk-volume change occurred (Figure 4a). These volume changes were systematically greater for the more densely compacted specimens. Water uptake and volume change in this range may result from a number of possible effects, including continued filling of the first H₂O layer, interstratification of multiple hydration states resulting from the presence of Ca²⁺ and Mg²⁺ in the exchange complex (36% and 4% of total CEC, respectively), partial disassociation of the quasicrystals resulting from adsorption on external surfaces, and adsorption in the larger intra-aggregate and inter-aggregate voids *via* surface hydration, electrical double layer development, or capillary condensation. In the latter case, the larger pores would either take on water without volume change or would expand as necessary to accommodate the additional water. If the total volume of the intra and inter-aggregate pores is limited (*e.g.* for a densely compacted specimen), then these pores would be more likely to expand, which is what was observed here. Expansion would also be expected to occur to a greater extent for the denser specimens, which was also evident in the results. RH ranging from ~60% to 80% for Na⁺-smectites marks transition from the one-layer to two-layer hydrate state, followed by a regime of relative stability, and then ultimate transition into a regime of interlayer dissociation *via* osmotic swelling. Each of the Wyoming bentonite specimens experienced significant increases in water content and volume within this range (Figures 3a, 4a). The change in interlayer spacing ($\Delta 2\delta$) for the one-layer to two-layer transition is comparable to that for the zero-layer to one-layer transition, yet the volume change results suggest that corresponding translation to bulk-

volume change is more efficient because the volume of the larger pores had been reduced to accommodate the previous zero-layer to one-layer transition.

In contrast to the Wyoming bentonite, the Colorado bentonite specimens (Figure 4b) exhibited more appreciable volume changes over the entire measured range. Volume change initiated immediately with the first RH increment and continued gradually thereafter, ultimately resulting in axial strains as high as 50% for the densely compacted specimen after the final RH increment. Results generally trend toward the denser preparations having larger volume changes, but the trend is more scattered than that for the Wyoming bentonite.

The immediate and more gradual volume change for the Colorado bentonite may be interpreted to reflect transition from the one-layer to two-layer hydration state. As noted in the XRD results (Figure 5b), the transition initiates at very low RH and occurs over a wide range. A corresponding increase in water content was noted in the sorption isotherms (Figure 3b) and in the volume change response for RH >~30% to 40%, where the XRD results would suggest a stable two-layer hydration state. These increases indicate that concurrent water uptake in the larger pore spaces via the mechanisms noted above is significant. For the two specimens compacted to similar density (Figure 4c), axial strain for the Colorado bentonite was 50–100% larger than for the Wyoming bentonite. The fact that volume changes are greater for the Colorado bentonite than for the Wyoming bentonite reflects the general differences in the microstructural features of predominantly divalent smectites and predominantly monovalent smectites. For example, previous SEM and TEM studies using monovalent smectites (*e.g.* Tessier, 1990) have shown that the microstructures of Ca²⁺, Na⁺, and Mg²⁺ smectites at low suction pressure (0.032 bar) and corresponding large water content are similar. The number of mineral layers making up quasicrystals within the clay aggregates, however, is generally larger for predominantly divalent cation systems than for predominantly monovalent cation systems and increases as the system dries, reaching as many as 400 face-to-face oriented layers for Ca²⁺-smectite and perhaps 20 layers for Na⁺-smectite at 1000 bar (~48% RH). Thus, for initially dry bentonites compacted to the same total void ratio, intra-aggregate voids forming the pore space among a network of relatively thin quasicrystals in a predominantly monovalent system may comprise a greater fraction of the total void volume than those formed among relatively thick quasicrystals in a divalent system. Interlayer volume changes would thus be expected to be more effectively adsorbed by the internal pore volume, which is what was observed here.

Swelling pressure under confined-swelling conditions

Equilibrium during the suite of swelling-pressure tests conducted under fully confined conditions typically

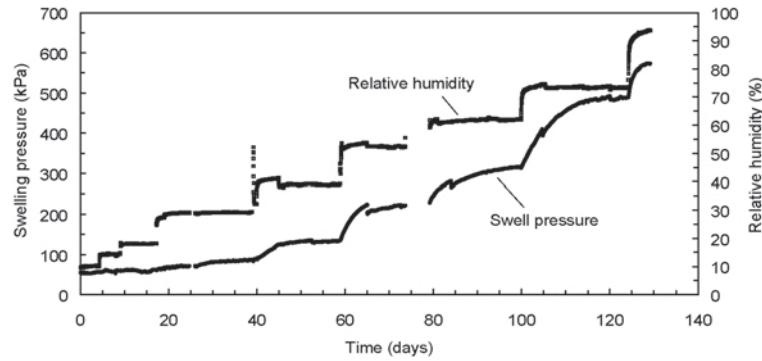


Figure 6. Example of transient RH and swelling pressure response from fully confined hydration of densely compacted ($e = 0.75$) Wyoming bentonite.

required 300 to 600 h (12.5 to 15 days) for each step (e.g. Figure 6). The amount of time to reach steady-state swelling pressure depended on the magnitude of the RH increment and the absolute magnitude of RH. More time was required for the increments where the change in swell pressure was greatest.

Steady-state swelling pressure for the Wyoming bentonite at RH values $< \sim 20\%$ did not increase significantly beyond the initial 40 kPa seating pressure for either the dense or loose specimen (Figure 7). Increases in swelling pressure with continuing hydration were very similar for the dense and loose preparations up to an RH of $\sim 50\%$. At higher RH, the swelling pressure response deviated and the more densely compacted specimen exhibited greater pressure. The dense and loose specimens exerted pressures of 573 kPa and 317 kPa at the final and largest RH increment of 97%.

In contrast, the response of the Colorado bentonite was more sensitive to compaction. Deviations in swelling pressure were apparent even at the first RH increment. The dense specimen exerted more pressure than the relatively loose specimen over the entire measured range. Both specimens also exhibited yielding or collapse behavior evident as a peak in the swelling pressure response. The dense and loose preparations reached peak pressures at ~ 1300 kPa and 550 kPa, respectively, with the peaks occurring at RH ranging from $\sim 50\%$ to 70%. Swelling pressures then decreased in both cases up to the final RH increment. Similar responses were not evident for the Wyoming bentonite over the measured range, but the swelling pressure for both the loose and dense preparations did appear to level off as RH approached 100%.

Plotting a derivative form of the response as the slope of the relationship between swelling pressure and relative humidity ($\Delta\sigma/\Delta RH$) provides additional perspective for interpreting these results (Figure 8). Generalized humidity regimes corresponding to basal-spacing transitions are shown as shaded regions on these figures. The derivative swelling pressure response for the densely compacted Wyoming bentonite (Figure 8a) shows peaks occurring near 70% RH and to a lesser

extent near 10% RH. The greater peak evident at 70% RH suggests that transition from the one- to two-layer interlayer hydration state was efficiently translated from the interlayer scale to the boundary of the specimen. The less well defined peak within the range of the zero-to-one layer transition suggests the initial interlayer swelling was more effectively absorbed by the surrounding void space and thus did not translate to external swelling pressure. As noted above, this was also observed in the volume change response for free swelling (Figure 4a) and from previous free swelling tests (Likos and Lu, 2006). The lack of similar peaks in the derivative response of the loosely compacted specimen suggests that both the zero-to-one and one-to-two layer transitions were not effectively translated to the bulk scale. The corresponding swelling pressure response was more gradual and the maximum pressure reached was relatively low (Figure 7). The derivative response for the Colorado bentonite (Figure 8b), on the other hand, indicated that the one-to-two layer transition was effectively translated to bulk swelling pressure.

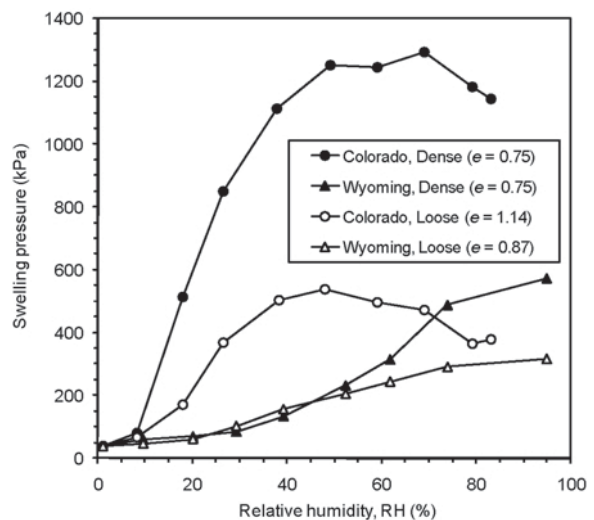


Figure 7. Steady-state swelling pressures measured from fully confined hydration tests.

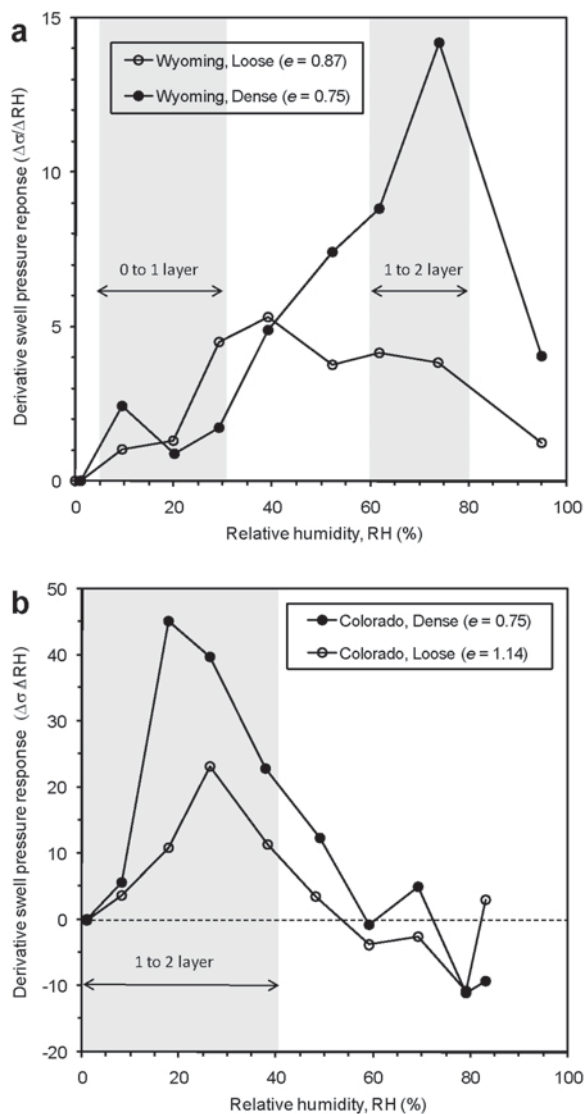


Figure 8. Derivative swelling pressure response as a function of RH from fully confined hydration tests.

Peaks in the derivative response are evident near 20% to 30% RH for both the dense and loose preparations. This suggests that the one-to-two layer transition was more efficiently translated to the specimen boundary for the dense specimen because the smaller volume of internal voids could not accommodate the interlayer swelling as effectively, ultimately resulting in greater swelling pressure after the basal-spacing transition was complete.

Interpretation of yielding behavior

The yielding (peak swelling pressure) behavior evident in the swelling pressure response of the Colorado bentonite (Figure 7) has been observed previously in a variety of suction-controlled hydration tests for compacted bentonites. For example, Lloret *et al.* (2003) reported results from constant-volume oedometer

tests conducted under humidity-controlled conditions for a predominantly divalent bentonite similar to the Colorado bentonite examined here [$w_1 = 102\%$; CEC = 111 meq/100 g comprising 38% Ca^{2+} , 28% Mg^{2+} , 23% Na^+ , and 2% K^+]. The results showed a peak in swelling pressure equal to ~ 1 MPa for a relatively loosely compacted specimen ($\gamma = 1.5 \text{ g/cm}^3$) and a peak at ~ 8.5 MPa for a relatively dense specimen ($\gamma = 1.65 \text{ g/cm}^3$). The corresponding RH at these peaks ranged from $\sim 77\%$ RH to 92% RH. Peak swelling pressure for a specimen compacted to $\gamma = 1.57 \text{ g/cm}^3$ was equal to ~ 2.2 MPa and occurred at RH of $\sim 90\%$. This is in close agreement with the similarly prepared dense specimen of Colorado bentonite reported here ($\gamma = 1.55 \text{ g/cm}^3$), which reached peak pressure of ~ 1.3 MPa at RH of $\sim 70\%$.

Yielding has also been observed in the transient swelling-pressure response of initially dry bentonites maintained under zero-volume-change conditions and fully immersed in water. Swelling pressure in such tests often increases almost immediately, reaches a first maximum soon after immersion (~ 1 – 2 days depending on specimen size), decreases, and then gradually increases to a second maximum as saturation is approached. For example, Schanz and Tripathy (2009) observed two swelling-pressure maxima in the transient response of a predominantly divalent bentonite compacted to relatively dense conditions (1.34 g/cm^3 and 1.56 g/cm^3) but not compacted to relatively loose conditions (1.12 g/cm^3 and 1.18 g/cm^3). Katti and Shanmugasundaram (2001) reported results for dry Wyoming bentonite (Natural Gel, Wyo-Ben, Inc.) compacted to loose initial conditions ($e = 2.14$). Swelling pressure reached a first peak at 120 kPa, decreased, and then gradually increased to a steady value of 163 kPa. Pusch (1982) observed similar behavior for compacted Wyoming Na^+ -bentonite (MX-80) hydrated from an initial water content of 10%. Komine and Ogata (1994) observed a peak in swelling pressure for Na^+ -bentonite compacted to $\gamma = 1.79 \text{ g/cm}^3$ at low initial moisture ($w = 6.3\%$) but not for a similar specimen compacted to greater density ($\gamma = 2.02 \text{ g/cm}^3$). Specimens compacted to 1.58 g/cm^3 and 1.89 g/cm^3 at greater water contents ($w = 19.8\%$ and $w = 17.2\%$) showed no peaks in the swelling-pressure response.

New perspective on the mechanisms leading to this type of yielding response is gained by considering the behavior to reflect transition from a wetting regime dominated by interlayer hydration to a wetting regime dominated by water uptake in the larger intra-aggregate and inter-aggregate pores. At greater RH, energies associated with hydration of the interlayer cations and surface sites are satisfied such that continued water uptake occurs via osmotic and capillary condensation processes in the larger pore groups. Condensation of liquid in the intra-aggregate pores results in forces that bring particles together within the aggregates, while

condensation occurring in the inter-aggregate pores results in forces that bring the aggregates themselves together. In either case, this promotes collapse of the aggregates and the matrix of aggregates, most notably if external stress is applied or if a zero-volume-change condition is imposed. This ultimately results in plastic compression of the fabric and a corresponding reduction in bulk swelling pressure such as that noted in Figure 7. If electrical double layers develop in the intra-aggregate and inter-aggregate pores, collapse may also be necessary to achieve particle separation distances that are in equilibrium with the corresponding osmotic pressure (Schanz and Tripathy, 2009), although this mechanism is probably more relevant at higher degrees of saturation achieved in full water immersion tests.

Considering the present results, it follows that the peak in swelling pressure was more evident and occurred at lower RH for the Colorado bentonite than for the Wyoming bentonite. If the predominantly divalent exchange complex of the former restricted interlayer hydration to two water layers and if this state was relatively stable for RH ranging from 40% to 90%, then any water adsorbed within this range would have been taken up in the larger intra- and inter-aggregate pores, leading to the potential collapse mechanisms described above. Considering the sorption results (Figure 3b), the amount of water adsorbed in this RH regime was appreciable in the case of free swelling, and has also been shown to be appreciable for similar bentonites hydrated under fully confined conditions (Villar, 2007). If water taken up in the larger pores contributes to their collapse, then the onset of collapse would be expected to coincide with the range of RH where water uptake in these pores becomes significant. The location of the peaks from 50% RH to 90% RH for the Colorado bentonite here and for the similar divalent bentonite of Lloret *et al.* (2003) are consistent with this range. The fact that the Wyoming bentonite did not show a clear peak in this range but swelling pressure did appear to level off as RH approached 100% reflects its capacity to continue to adsorb interlayer water even at high RH. Continued water uptake beyond the two or three water layers at ~90% RH occurs both in the interlayer and the larger pores, whereupon collapse of the larger pores may occur. This ultimately leads from a bimodal pore size to a single pore size if wetting occurs under high confining stress or zero-volume-change boundary conditions (*e.g.* Romero and Simms, 2008) or to the formation of a dispersed gel if wetting occurs under free swelling conditions.

Porosity evolution modeling

Likos and Lu (2006) proposed a pore-scale framework to quantitatively assess the evolution of expansive clay microstructure and macrostructure resulting from interlayer hydration. In this section, that framework is applied to interpret results from the current tests conducted under zero-volume-change boundary condi-

tions. Focus is placed on analyzing results obtained for densely compacted specimens of Colorado and Wyoming bentonite ($e = 0.75$) so that comparisons may be made with previous modeling results for similarly compacted ($e = 0.77$) specimen tests under free swelling conditions (Likos and Lu, 2006).

As noted in Figure 1b, total pore volume is considered to reside on two levels of scale and written in terms of void ratio as

$$e_t = e_{ip} + e_{il} \quad (1)$$

where e_t is total void ratio, e_{ip} is an interparticle void ratio, and e_{il} is an interlayer void ratio. The interlayer void ratio may be quantified from the ratio of total interlayer volume (V_{il}) to the total solids volume (V_s), which can be reduced to the ratio of an interlayer separation distance (2δ) and the thickness of the mineral sheet (τ):

$$e_{il} = \frac{V_{il}}{V_s} = \frac{2\delta}{\tau} \quad (2)$$

or considering equation 1

$$e_t = e_{ip} + \frac{2\delta}{\tau} \quad (3)$$

The interlayer separation distance (2δ) varies with changing RH, whereas mineral sheet thickness is a constant ($\tau = 9.70 \text{ \AA}$). The interlayer void ratio may be calculated from interlayer separation distance as a function of RH, which may be estimated by assigning RH ranges for the transition and stability of various interlayer hydration states. Thus, equation 3 may be written in an incremental form to quantify the change in total void ratio that results from coupled changes in the interparticle and interlayer void volumes:

$$\Delta e_t = \Delta e_{ip} + \frac{\Delta 2\delta}{\tau} \quad (4)$$

For tests conducted under free-swelling conditions, the total void ratio may be computed from the measured specimen volume (axial strain) and gravimetric water content. For tests conducted under zero-volume-change conditions, the total void ratio remains a constant equal to that initially imposed by compaction. The interparticle void ratio is equal to the difference in the total and interlayer void ratios by equation 4. Changes in interparticle void ratio may be either positive or negative, where the latter case reflects a loss of pore volume that occurs as expanding interlayers encroach into the surrounding pores. Positive changes in interparticle void ratio reflect an expansion of the pores as necessary to accommodate water uptake or to come to equilibrium with repulsive interparticle forces that may develop. For fully confined specimens, the total void ratio may not change and any increases in interlayer void volume must be offset by an equivalent decrease in interparticle void volume.

The suite of XRD measurements in Figure 5 was used to establish representative trend lines for basal spacing as a function of RH (denoted by bold dashed lines). Corresponding evolution of interlayer and interparticle void ratio was plotted for the Wyoming bentonite (Figure 9a) and the Colorado bentonite (Figure 9b) under free and fully confined swelling conditions. Interlayer void ratio (solid circles) for the Wyoming bentonite was computed from the trend line in Figure 5a and shows transitions through the zero-layer, one-layer, and two-layer hydration states. Interlayer void ratio for the Colorado bentonite was computed from the trend line in Figure 5b and shows transition from the initial one-layer hydration state to the two-layer hydration state by RH of 40%. Open circles show the interparticle void ratio modeled under zero-volume-change conditions computed using the fixed total void ratios ($e_t = 0.75$) and equation 4. Open triangles show interparticle void ratios computed for similarly compacted specimens ($e_t = 0.77$) under free-swelling conditions.

The modeled interparticle void ratio decreased in a similar way during the zero-to-one layer transition for the free and confined Wyoming bentonite specimens (Figure 9a). In both cases, the interparticle volume decreased from initially 100% of the total void volume to

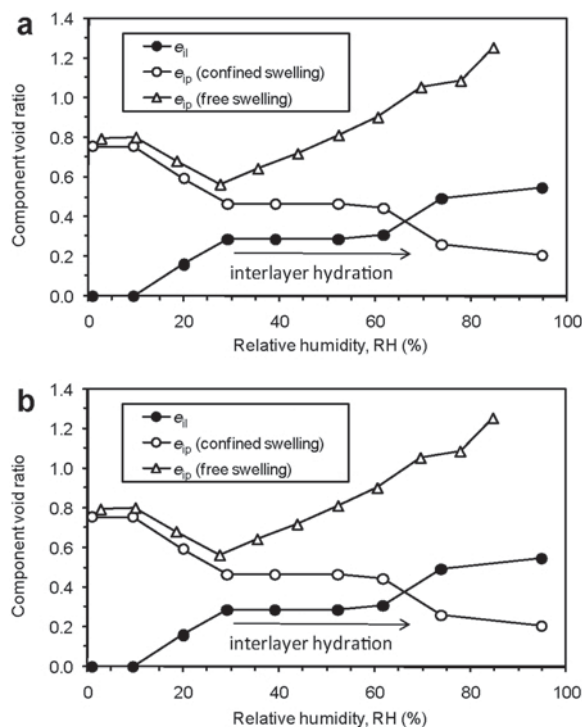


Figure 9. Modeled evolution of interlayer (e_{il}) and interparticle (e_{ip}) void ratio for free and confined swelling tests: (a) Wyoming bentonite and (b) Colorado bentonite. Specimens for confined swelling tests were compacted to an initial total void ratio of 0.75. Specimens for free swell tests (Likos and Lu, 2006) were compacted to an initial total void ratio of 0.77.

~66%. The ratio of interlayer void volume to interparticle void volume increased from 0% to 51%. As noted above, this reduction of the larger-scale pore volume did not translate into swelling pressure for the confined specimen, nor did it translate into volume change for the unconfined specimen. The modeled interparticle void ratio for the unconfined specimen from ~30% RH to ~60% RH increased significantly. This suggests an expansion of the larger pores that may have been necessary to accommodate the water adsorbed within this range or to come to equilibrium with repulsive forces from double layers developing among the larger particle groups. The modeled interparticle void ratio for the confined specimen over the same range was stable because the interlayer void ratio was stable and because the specimen did not change the total volume. The swelling pressure within this range, however, increased from ~100 kPa to 300 kPa, suggesting that water uptake occurred in the interparticle pores and that constraint on expansion of these pores resulted in swelling pressure measurable at the specimen boundary. The RH from ~60% to ~80% marked transition from the one-layer to the two-layer hydrate state. In the case of free swelling, concurrent expansion of the interparticle voids occurred and resulted in significant bulk-volume change. The interparticle void volume for the confined specimen decreased to accommodate the transition, which resulted in a large increase in swelling pressure. The increase in swelling pressure was more appreciable for this interlayer transition than for the first (Figure 8a) because the volume of the interparticle voids prior to the transition was much smaller.

Modeling results for the Colorado bentonite (Figure 9b) are quite different. The interlayer void volume initially represented 42% of the total void volume because testing commenced from the one-layer hydration state. The corresponding interparticle void volume was 58% of the total void volume. Transition from the one-layer to two-layer hydration state for the confined specimen resulted in expansion of the particles into the surrounding voids. This decreased the interparticle void volume from an already relatively small 58% to 30% of the total void volume. The reduction caused an immediate and efficient translation to bulk swelling pressure (Figure 7) and a well defined peak in the derivative swelling pressure response (Figure 8). The unconfined specimen during the one-to-two layer transition showed a similarly efficient translation to bulk-volume change accompanied by a concurrent increase in the interparticle void volume. The modeled interlayer void volume for RH from ~40% to 90% was stable, and thus the interparticle void ratio for the confined specimen remained stable. Water uptake in these voids may have resulted in adjustments to their structure and a corresponding relaxation of swelling pressure. The total volume of the unconfined specimen increased considerably in the same range as the volume of the interparticle pores increased to accommodate the water being adsorbed.

SUMMARY AND CONCLUSIONS

The mechanical behavior of compacted bentonite within the interlayer swelling regime was examined *via* controlled-humidity sorption tests conducted under free-swelling and confined-swelling conditions. Emphasis was placed on examining the influences of compaction density and predominant exchange cation (Na^+ vs. $\text{Ca}^{2+}/\text{Mg}^{2+}$) on measured sorption, volume change, and swelling pressure response. Water-vapor sorption behavior for both bentonites was essentially independent of compaction density for RH $< 95\%$. Volume changes measured under free-swelling conditions and swelling pressures measured under fully confined conditions, on the other hand, were dependent on compaction density. Densely compacted specimens exhibited both greater volume changes and greater swelling pressures. Relatively low density and low confining stress conditions created an environment conducive to a more open fabric and a larger volume of intra-aggregate and inter-aggregate voids such that interlayer expansion was more effectively decoupled from volume changes and swelling pressures measurable at the specimen boundary. Relatively high density and high confining-stress conditions created an environment conducive to a more closed fabric, such that interlayer expansion was more efficiently translated to measurable bulk response. New perspective into the yielding response of bentonites hydrated under confined conditions was obtained by illustrating that yielding may correspond to transition from a wetting regime dominated by interlayer hydration to a regime dominated by water uptake into larger scale pore groups. Yielding was shown to be more significant and to occur earlier for Colorado ($\text{Ca}^{2+}/\text{Mg}^{2+}$) bentonite than for Wyoming (Na^+) bentonite, observations interpreted to reflect the limited capacity for interlayer swelling in the former. Semi-quantitative analysis of porosity evolution showed that interlayer-volume change resulting from the zero-to-one layer transition in basal spacing for Wyoming bentonite was effectively absorbed internally by the larger-scale pores. Corresponding bulk-volume change and swelling pressure were insignificant. The one-to-two layer transition was more effectively translated into volume change and swelling pressure because the volume of larger-scale voids had been reduced. The one-to-two layer transition for Colorado bentonite was less efficiently accommodated by the larger voids, resulting in much larger changes in volume and swelling pressure.

ACKNOWLEDGMENTS

Acknowledgment is made to the Donors of the American Chemical Society Petroleum Research Fund for partial support of this research. The authors are indebted to the three anonymous reviewers and

Associate Editor, Reiner Dohrmann, whose detailed review comments significantly improved the manuscript.

REFERENCES

- Al-Mukhtar, M., Qi, Y., Alcover, J.F., and Bergaya, F. (1999) Oedometric and water-retention behavior of highly compacted unsaturated smectites. *Canadian Geotechnical Journal*, **36**, 675–684.
- Alonso, E.E., Vaunat, J., and Gens, A. (1999) Modeling the mechanical behavior of expansive clays. *Engineering Geology*, **54**, 173–183.
- ASTM (2000) ASTM D4318-05 Standard Test Methods for Liquid Limit, Plastic Limit, and Plasticity Index of Soils, ASTM International, 4.08, West Conshohocken, Pennsylvania, USA.
- Aylmore, L.A.G. and Quirk, J.P. (1971) Domains and quasicrystalline regions in clay systems. *Soil Science Society of America Proceedings*, **35**, 652–654.
- Berend, I., Cases, J., Francois, M., Uriot, J., Michot, L., Maison, A., and Thomas, F. (1995) Mechanism of adsorption and desorption of water vapor by homoionic montmorillonites. *Clays and Clay Minerals*, **43**, 324–336.
- Bernier, F., Volckaert, G., Alonso, E., and Villar, M. (1997) Suction-controlled experiments on Boom clay. *Engineering Geology*, **47**, 325–338.
- Caballero, E., Jimenez de Cisneros, C., and Linares, J. (2004) Physicochemical properties of bentonite: effect of the exchangeable cations. Pp. 40–47 in: *FEDEX II Project. THG Laboratory Experiments* (T. Missana, editor). Publicacion Tecnica ENRESA 09/2004, Madrid.
- Cases, J.M., Berend, I., Besson, G., Francois, M., Uriot, J.P., Thomas, F., and Poirier, J.E. (1992) Mechanism of adsorption and desorption of water vapor by homoionic montmorillonite. I. The sodium exchanged form. *Langmuir*, **8**, 2730–2739.
- Cases, J.M., Berend, I., Besson, G., Francois, M., Uriot, J.P., Michot, L., and Thomas, F. (1997) Mechanism of adsorption and desorption of water vapor by homoionic montmorillonite. III. The Mg^{2+} , Ca^{2+} , Sr^{2+} , and Ba^{2+} exchanged forms. *Clays and Clay Minerals*, **45**, 8–22.
- Chipera, S.J., Carey, J.W., and Bish, D.L. (1997) Controlled-humidity XRD analyses: Application to the study of smectite expansion/contraction. Pp. 713–721 in: *Advances in X-ray Analysis*, 36 (J.V. Gilfrich *et al.*, editors). Plenum Press, New York.
- Cui, Y.J., Yahia-Aissa, M., and Delage, P. (2002) A model for the volume change behavior of heavily compacted swelling clays. *Engineering Geology*, **64**, 233–250.
- Delage, P., Howat, M.D., and Cui, Y.J. (1998) The relationship between suction and swelling properties in a heavily compacted unsaturated clay. *Engineering Geology*, **50**, 31–48.
- Del Pennino, U., Mazzega, E., and Valeri, S. (1981) Interlayer water and swelling properties of monoionic montmorillonites. *Journal of Colloid and Interface Science*, **84**, 301.
- Devineau, K., Bihannic, I., Michot, L., Villieras, F., Masrouri, F., Cuisinier, O., Fragneto, G., and Michau, N. (2006) In situ neutron diffraction analysis of the influence of geometric confinement on crystalline swelling of montmorillonite. *Applied Clay Science*, **31**, 76–84.
- Dohrmann, R. and Kauffhold, S. (2009) Three new, quick CEC methods for determining the amounts of exchangeable calcium cations in calcareous clays. *Clays and Clay Minerals* **57**, 338–352.
- Eberl, D.D., Drits, V.A., and Środoń, J. (1996) *MUDMASTER; a program for calculating crystallite size distributions and*

- strain from the shapes of X-ray diffraction peaks. US Geological Survey Open File Report 96-0171.
- Ferrage, E., Lanson, B., Sakharov, B.A., and Drits, V.A. (2005) Investigation of smectite hydration properties by modeling experimental X-ray diffraction patterns: Part I. Montmorillonite hydration properties. *American Mineralogist*, **90**, 1358–1374.
- Fripiat, J.T., Jelli, A., Poncelet, G., and Andre, J. (1965) Thermodynamic properties and adsorbed water molecules and electrical conduction in montmorillonite and silicates. *Journal of Physical Chemistry*, **69**, 2185–2197.
- Gens, A. and Alonso, E.E. (1992) A framework for the behavior of unsaturated expansive clays. *Canadian Geotechnical Journal*, **29**, 1013–1032.
- Gillery, F.H. (1959) Adsorption-desorption characteristics of synthetic montmorillonoids in humid atmospheres. *American Mineralogist*, **44**, 806.
- Hall, P.L. and Astill, D.M. (1989) Adsorption of water by homoionic exchange forms of Wyoming montmorillonite (Swy-1). *Clays and Clay Minerals*, **37**, 355–363.
- Hashizume, H., Shimomura, S., Yamada, H., Fujita, T., Nakazawa, H., and Akutsu, O. (1996) X-ray diffraction system with controlled relative humidity and temperature. *Powder Diffraction*, **11**, 288–289.
- Huang, W., Bassett, W.A., and Wu, T. (1994) Dehydration and hydration of montmorillonite at elevated temperatures and pressures monitored using synchrotron radiation. *American Mineralogist*, **79**, 683–691.
- Katti, D.R. and Shanmugasundaram, V. (2001) Influence of swelling on the microstructure of expansive clays. *Canadian Geotechnical Journal*, **38**, 175–182.
- Keren, R. and Shainberg, I. (1975) Water vapor isotherms and heat of immersion of Na/Ca-montmorillonite systems – I: Homoionic clay. *Clays and Clay Minerals*, **23**, 193–200.
- Keren, R. and Shainberg, I. (1979) Water vapor isotherms and heat of immersion of Na/Ca-montmorillonite systems – II: Mixed Systems. *Clays and Clay Minerals*, **27**, 145–151.
- Keren, R. and Shainberg, I. (1980) Water vapor isotherms and heat of immersion of Na/Ca-montmorillonite systems – III: Thermodynamics. *Clays and Clay Minerals*, **28**, 204–210.
- Komine, H. and Ogata, N. (1994) Experimental study on swelling characteristics of compacted bentonite. *Canadian Geotechnical Journal*, **31**, 478–490.
- Laird, D.A., Shang, C. and Thompson, M.L. (1995) Hysteresis in crystalline swelling of smectites. *Journal of Colloid and Interface Science*, **171**, 240–245.
- Lambe, T.W. and Whitman, R.V. (1969) *Soil Mechanics*. Wiley, New York.
- Likos, W.J. (2004) Measurement of crystalline swelling in expansive clay. *Geotechnical Testing Journal*, **27**, 540–546.
- Likos, W.J. and Lu, N. (2006) Pore-scale analysis of bulk volume change from crystalline swelling in Na⁺- and Ca²⁺-smectite. *Clays and Clay Minerals*, **54**, 516–529.
- Lloret, A., Villar, M.V., Sánchez, M., Gens, A., Pintado, X., and Alonso, E.E. (2003) Mechanical behavior of heavily compacted bentonite under high suction changes. *Géotechnique*, **53**, 27–40.
- Mooney, R.W., Keenan, A.G., and Wood, L.A. (1952) Adsorption of water vapor by montmorillonite. II. Effect of exchangeable ions and lattice swelling as measured by X-ray diffraction. *Journal of the American Chemical Society*, **74**, 1371–1374.
- Moore, D.M. and Reynolds, R.C. (1997) *X-ray Diffraction and the Identification and Analysis of Clay Minerals*. Oxford University Press, New York.
- Noe, D.C., Higgins, J.D., and Olsen, H.W. (2007) Steeply dipping heaving bedrock, Colorado: Part 2 – Mineralogical and Engineering Properties. *Environmental and Engineering Geoscience*, **XIII**, 309–324.
- Norrish, K. (1954) The swelling of montmorillonite. *Transactions of the Faraday Society*, **18**, 120–134.
- Ormerod, E.C. and Newman, A.C.D. (1983) Water sorption on Ca-saturated clays: II. Internal and external surfaces of montmorillonite. *Clay Minerals*, **18**, 289–299.
- Pusch, R. (1982) Mineral-water interactions and their influence on the physical behavior of highly compacted Na bentonite. *Canadian Geotechnical Journal*, **19**, 381–387.
- Pusch, R. (1994) *Waste Disposal in Rock*. Developments in Geotechnical Engineering, 76. Elsevier, Amsterdam, 490 pp.
- Romero, E. and Simms, P.H. (2008) Microstructure investigation in unsaturated soils: A review with special attention to contribution of mercury intrusion porosimetry and environmental scanning electron microscopy. *Geotechnical and Geological Engineering*, **26**, 705–727.
- Saiyouri, N., Tessier, D., and Hicher, P.Y. (2004) Experimental study of swelling in unsaturated compacted clays. *Clay Minerals*, **39**, 469–479.
- Sánchez, M., Gens, A., Guimarães, L.N., and Olivella, S. (2005) A double structure generalized plasticity model for expansive materials. *International Journal for Numerical and Analytical Methods in Geomechanics*, **29**, 751–787.
- Schanz, T. and S. Tripathy (2009) Swelling pressure of a divalent-rich bentonite: Diffuse double-layer theory revisited. *Water Resources Research*, **45**, W00C12.
- Tessier, D. (1990) Behavior and microstructure of clay minerals. Pp. 387–415 in: *Soil Colloids and their Associations in Aggregates* (M.F. DeBoodt *et al.*, editors). Plenum Press, New York.
- Tuller, M. and Or, D. (2003) Hydraulic functions for swelling soils: pore-scale considerations. *Journal of Hydrology*, **272**, 50–71.
- USDA (2004) *Soil Survey Laboratory Methods Manual*, Soil Survey Investigations Report No. 42, R. Burt (editor). United States Department of Agriculture, method 4B1b, Version 4.0, 2004.
- Villar, M.V. (1999) Investigation of the behavior of bentonite by means of suction-controlled oedometer tests. *Engineering Geology*, **54**, 67–73.
- Villar, M.V. (2007) Water retention of two natural compacted bentonites. *Clays and Clay Minerals*, **55**, 311–322.
- Yahia-Aissa, M., Delage, P., and Cui, Y.J. (2001) Suction-water content relationship in swelling clays. Pp. 65–68 in: *Clay Science for Engineering* (K. Adachi and M. Kukue, editors). Balkema, Rotterdam.
- Young, J.F. (1967) Humidity control in the laboratory using salt solutions – A review. *Journal of Applied Chemistry*, **17**, 241–245.
- Zettlemayer, A.C., Young, E.J., and Chessick, J.J. (1955) Studies of the surface chemistry of silicate minerals – III. Heat of immersion of bentonite in water. *Journal of Physical Chemistry*, **59**, 962–966.

(Received 10 July 2009; revised 15 March 2010; Ms. 338; A.E. R. Dohrmann)